Excited-State Structure and Dynamics of *cis*- and *trans*-Azobenzene from Resonance Raman Intensity Analysis

Christina M. Stuart, Renee R. Frontiera, and Richard A. Mathies*

Department of Chemistry, University of California at Berkeley, Berkeley, California 94720

Received: July 2, 2007; In Final Form: September 13, 2007

Resonance Raman intensity analysis was used to investigate the initial excited-state nuclear dynamics of *cis*- and *trans*-azobenzene following S_1 ($n\pi^*$) excitation, and fluorescence quantum yield measurements were used to estimate the excited-state lifetimes. *trans*-Azobenzene exhibits the strongest Raman intensities in its skeletal stretching and bending modes, while torsional motions dominate the nuclear relaxation of *cis*-azobenzene as indicated by intense Raman lines at 275, 542, 594, and 778 cm^{-1}. The very weak fluorescence quantum yield for *cis*-azobenzene is consistent with its ∼100 fs electronic lifetime while *trans*-azobenzene, with a fluorescence quantum yield of 1.1×10^{-5}, has an estimated S_1 lifetime of ∼3 ps. The absorption and Raman cross-sections of both isomers were modeled to produce a harmonic displaced excited-state potential energy surface model revealing the initial nuclear motions on the reactive surface, as well as values for the homogeneous and inhomogeneous linewidths. For *cis*-azobenzene, this modeling predicts slopes on the S_1 potential energy surface that when extrapolated to the position of the harmonic minimum give excited-state changes of ∼6−20° in the CNNC torsion angle and a ≤3° change in the CNN bending angle. The relatively large excited-state displacements along these torsional degrees of freedom provide the driving force for ultrafast isomerization. In contrast, the excited-state geometry changes of *trans*-azobenzene are primarily focused on the CNN bend and CN and NN stretches. These results support the idea that *cis*-azobenzene isomerizes rapidly via rotation about the NN bond, while isomerization proceeds via inversion for *trans*-azobenzene.

1. Introduction

Azobenzene is an attractive molecular transducer for light-driven devices and optical switches due to the large but reversible changes in its electronic dipole and molecular shape that occur upon isomerization.[1] Azobenzene has been used to develop optical storage devices,[2] to regulate ion channels in the ligand-binding domain of proteins,[3] and to control the interconversion between peptide conformations.[4,5] These light-driven applications are facilitated by the distinct absorption bands of the cis and trans isomers that allow for selective conversion and are robust even after multiple photocycles.[1,3,4,6] However, the isomerization quantum yields are below 60%,[7−9] and there is still considerable debate regarding the mechanisms and rates of the isomerization process. Studies aimed at determining the isomerization mechanism and dynamics of azobenzene are needed to understand and optimize its photoswitching capabilities.

trans-Azobenzene is planar in the ground state with an absorption spectrum consisting of a strongly allowed transition to S_2 ($\epsilon_{317} = 16\,980\ M^{-1}\ cm^{-1}$, photoisomerization quantum yield $\phi_{t\rightarrow c} = 0.10$) and a weakly allowed transition to S_1 ($\epsilon_{449} = 405\ M^{-1}\ cm^{-1}$, $\phi_{t\rightarrow c} = 0.25$).[7,8] In contrast, the ground state of *cis*-azobenzene has a CNNC dihedral angle of 10°.[10−13] The absorption spectrum of *cis*-azobenzene exhibits a moderate S_2 band at ∼290 nm ($\epsilon = 4980\ M^{-1}\ cm^{-1}$, $\phi_{c\rightarrow t} = 0.27$) and a weaker S_1 transition at 434 nm ($\epsilon = 1295\ M^{-1}\ cm^{-1}$, $\phi_{c\rightarrow t} = 0.56$).[7,9] The greater absorption cross-section for the S_1 band in *cis*-azobenzene as compared to that of *trans*-azobenzene is likely due to intensity borrowing from the allowed transition as a result of the nonplanarity of the molecule.[1] Conversion between the isomers can take place via torsion about the NN bond, similar to the mechanism observed in stilbene,[14] or via inversion analogous to the isomerization of imines.[15]

To understand the isomerization mechanism and dynamics of *trans*-azobenzene, extensive theoretical and experimental studies have been performed. The measured S_1 lifetime of *trans*-azobenzene ranges from 1 to 30 ps and is solvent-dependent.[16−21] Until recently, isomerization of *trans*-azobenzene was generally thought to proceed via inversion when excited into S_1.[17,18,22] This conclusion was supported by studies of rotationally hindered azobenzene derivatives that maintained the same isomerization quantum yields despite elimination of the rotational pathway.[8] Additionally, Raman intensity calculations have indicated that the early time dynamics in S_1 are along the inversion coordinate,[23] and ab initio calculations have also suggested inversion to be the dominant pathway.[24,25] However, isomerization via inversion has recently been challenged by a number of independent calculations that favor rotation because it is barrierless and has an S_0/S_1 curve crossing at a CNNC angle of ∼90°.[26−31] In contrast, the inversion coordinate is predicted to have a 9.6 kcal/mol barrier, and the S_0 and S_1 surfaces do not cross.[31] Recent femtosecond anisotropy measurements also suggest that the rotational pathway is dominant in nonviscous solvents, such as *n*-hexane.[21] However, fluorescence up-conversion and calculations suggest that the inversion coordinate becomes dominant for rotationally hindered azobenzenes.[29,32]

In contrast to the trans isomer, *cis*-azobenzene isomerizes on the femtosecond time scale, making direct observation of the dynamics more challenging. However, femtosecond transient absorption studies have measured the S_1 lifetime to be ∼100−

* Corresponding author. E-mail: rich@zinc.cchem.berkeley.edu; phone: (510) 642-4192; fax: (510) 642-3599.

10.1021/jp0751460 CCC: $37.00
Published on Web 11/07/2007

170 fs,[17,20] consistent with the short excited-state lifetime obtained from simulations employing surface hopping and full multiple spawning methods.[30] Additionally, CASSCF ab initio and time-dependent density functional theory calculations have found that the S_1 potential energy surface in the Franck−Condon (FC) region is steep and barrierless along the rotational coordinate.[26,31] Few spectroscopic studies investigating the isomerization mechanism have been performed on *cis*-azobenzene, and the majority of the mechanistic information has been obtained from calculations.

Here, we present a quantitative comparison and analysis of resonance Raman spectra of *trans*- and *cis*-azobenzene with the goal of determining the coordinate along which the initial reaction dynamics occur. The absolute resonance Raman cross-sections of both isomers are reported, and vibronic analysis was performed to develop a complete FC synthesis of the excited-state vibrational structure and homogeneous and inhomogeneous linewidths. Additionally, the fluorescence spectra were measured, and Strickler−Berg analysis was used to estimate the S_1 excited-state lifetime of *trans*- and *cis*-azobenzene. These results are critically compared with the various models for excited-state isomerization dynamics of *cis*- and *trans*-azobenzene.

2. Materials and Methods

Solutions of azobenzene (Sigma, 99%) prepared in ethanol (Aldrich, 99% anhydrous) consisted of a mixture of the trans and cis isomers. *cis*-Azobenzene was prepared in a darkroom by irradiating the solution containing a mixture of isomers on ice with a Blak-Ray long-wave UV lamp (365 nm) until the absorption max shifted from 317 to ∼306 nm, indicating that a majority of azobenzene was in the cis configuration. Using known extinction coefficients for each isomer at 317 and 434 nm ($\epsilon_{317} = 2520$ M^{-1} cm^{-1} and $\epsilon_{434} = 1295$ M^{-1} cm^{-1} for *cis*-azobenzene and $\epsilon_{317} = 16\,980$ M^{-1} cm^{-1} and $\epsilon_{434} = 400$ M^{-1} cm^{-1} for *trans*-azobenzene in ethanol),[1] concentrations of each isomer were determined. Samples produced by this method were ∼80% cis and ∼20% trans. Samples prepared by dissolving solid azobenzene in ethanol had a composition that was ∼80% trans and ∼20% cis and did not change when left at room temperature or exposed to room light.

For Raman experiments, 0.2−0.5 mM solutions of azobenzene were recirculated with a peristaltic pump through a 1.1−1.4 mm i.d. capillary at a rate of 3 mL/s to yield a photoalteration parameter, F, of <0.05 using quantum yields of 0.45 and 0.36 for cis and trans excited in the S_1 band and the illumination conditions defined next.[7] Solutions of *cis*-azobenzene were kept on ice and illuminated with a UV lamp during spectral acquisition to maintain the 80% cis composition. The temperature of the solution at the optical sampling point was ∼10 °C. Thermal cis → trans isomerization did not occur over the course of the experiment due to the long half-life of cis in the dark (96 h at room temperature).[33] Additionally, heating of the sample due to the laser was not expected to drive the thermal cis → trans isomerization because the thermal barrier is significant (∼20−27 kcal/mol),[34] and the samples flowed rapidly.

2.1. Optical System. Continuous excitation at 406, 458, 488, and 496 nm was obtained with an Ar^+ or Kr^+ laser; the focused beam at the sample had a diameter of 60 μm and a power of ∼2 mW. Scattering was collected at 90° and focused onto the entrance slit of a Spex 1401 double spectrograph. The dispersed light (8 cm^{-1} resolution at 800 nm) was imaged on a liquid nitrogen cooled CCD (Roper Scientific LN/CCD 1100). All spectra were corrected for the instrument response and self-absorption effects. Self-absorption corrections were determined by comparison of the solvent peak intensities in the presence and absence of azobenzene.

To measure the fluorescence spectra of *cis*- and *trans*-azobenzene, samples were prepared in the 0.2−0.5 mM range (OD = 0.03 at the sample point) and recirculated through a 1.1−1.4 mm i.d. capillary with a flow rate of ∼2 mL/s. Fluorescence spectra with excitation at 458 nm (∼3.5 mW) were collected at 90° and detected with a scanning double monochromator (Spex 1401) and photomultiplier. The entrance and exit slits were 400 μm, resulting in a 10 cm^{-1} spectral bandpass. Spectra were acquired in 10 cm^{-1} steps with 2 s accumulation time per point.

2.2. Resonance Raman Intensity Analysis. Absolute Raman cross-sections for *cis*- and *trans*-azobenzene were determined as described previously.[35] Briefly, the integrated areas of the azobenzene peaks were compared to the integrated area of a standard band (ethanol's CO stretch band at 881 cm^{-1}, $\partial\sigma_{std}/\partial\Omega = 3.00 \times 10^{-14}$ Å^2/molecule/steradian at 488 nm excitation).[36] The differential cross-section for the ethanol CO stretch at all excitation wavelengths was determined by extrapolating from the measured value at 488 nm, assuming that the scattering cross-section was proportional to $\nu_S{}^3\nu_L$, where ν_S and ν_L are the frequencies of scattered and laser light, respectively, and are given in Table 3. The differential cross-section of the standard band is related to the absolute Raman cross-sections of azobenzene by eq 1:

$$\sigma_{azo} = \frac{8\pi}{3}\frac{(1+2\rho)}{(1+\rho)}\left[\left(\frac{\nu_L - \nu_{azo}}{\nu_L - \nu_{std}}\right)^3\left(\frac{A_{azo}}{A_{std}}\right)\left(\frac{c_{std}}{c_{azo}}\right)\left(\frac{\partial\sigma_{std}}{\partial\Omega}\right)_{\parallel+\perp}\right] \quad (1)$$

where ν_{azo} and ν_{std} are the vibrational frequencies of azobenzene and the ethanol standard band, A_{azo} and A_{std} are the integrated areas, and c_{std} and c_{azo} are the concentrations for ethanol and azobenzene. The depolarization ratios, ρ, for all bands of both azobenzene isomers in ethanol were measured and found to be 1/3, as expected.

Raman excitation profiles (REPs) were calculated using the time-dependent wave packet formalism of resonance Raman (RR) intensities.[37] The absorption cross-section, σ_A, is determined by a Fourier transform of the overlap of the initial vibrational wavefunction propagating on the excited-state surface, $|i(t)\rangle$, with the stationary initial state $|i\rangle$ (eq 2), and the Raman cross-sections, σ_R, are determined by the square of the half-Fourier transform of the overlap of the final stationary vibrational state $|f\rangle$ with $|i(t)\rangle$ (eq 3):

$$\sigma_A = \frac{8\pi E_L e^2 M^2}{6\hbar^2 cn(\theta\sqrt{2\pi})}\int_0^\infty dE \times \exp\left[\frac{-(E-E_0)^2}{2\theta^2}\right]\mathrm{Re}\int_0^\infty dt\langle i|i(t)\rangle e^{-\Gamma_G{}^2t^2/\hbar^2}e^{i(E_L+\epsilon_i)t/\hbar} \quad (2)$$

$$\sigma_R = \frac{8\pi E_S{}^3 E_L e^4 M^4}{9\hbar^6 c^4(\theta\sqrt{2\pi})}\int_0^\infty dE \times \exp\left[\frac{-(E-E_0)^2}{2\theta^2}\right]\left|\int_0^\infty dt\langle f|i(t)\rangle e^{-\Gamma_G{}^2t^2/\hbar^2}e^{i(E_L+\epsilon_i)t/\hbar}\right|^2 \quad (3)$$

where E_L and E_S refer to the frequency of the laser and scattered radiation in centimeters^{-1}, M is the transition dipole in angstroms, E_0 is the zero−zero energy in centimeters^{-1}, ϵ_i is the vibrational energy of eigenstate i, Γ_G is the Gaussian homogeneous line width, and θ is the inhomogeneous broadening. The time-dependent overlaps depend parametrically upon

a set of dimensionless displacements (Δ) between the ground and the excited states along the normal coordinates that are coupled to the electronic transition.

Raman intensity calculations were carried out to model the experimental data by initially entering estimates of the relative deltas obtained from the intensities of the observed vibrational bands assuming $I \propto \Delta^2$. The overall scaling of Δ, homogeneous broadening Γ_G, inhomogeneous broadening θ, zero−zero energy E_0, and transition dipole M were then adjusted to provide the best fit to the overall shape of the absorption spectra and resonance Raman cross-sections.

The Δ values obtained from these calculations can be used to determine the excited-state Cartesian displacement along a specific internal coordinate from the following equation:[38]

$$\delta_i = 5.8065 \sum_j A_{ji} \omega_j^{-1/2} \Delta_j \tag{4}$$

where δ_i is the ground- to excited-state geometry change along internal coordinate i with units of angstroms for bond length changes and degrees for angle changes; A_{ji} is an element of the matrix relating the normal coordinates, j, to the internal coordinate basis set, i; ω_j is the frequency of the normal mode; and Δ_j is the dimensionless displacement along a normal coordinate j. Optimization and frequency calculations using Gaussian 03[39] for each of the isomers yielded a basis set of normal modes. Elements of the A_{ji} matrix were determined by conversion of the displacements from the normal mode basis set to an internal coordinate basis set.

2.3. Determination of Fluorescence Quantum Yield. The absolute fluorescence intensity of azobenzene was determined by comparison of the integrated area of the azobenzene fluorescence spectrum to that of the ethanol CH stretch bands. The absolute Raman cross-section, σ_{std}, for the CH stretch (2880 cm^{-1} band) was 1.5×10^{-12} A^2/molecule at 488 nm excitation.[36] Using the CH stretch of ethanol as a standard, the fluorescence quantum yield, Φ_{fl}, of *cis*- and *trans*-azobenzene can be determined from the following equation:

$$\Phi_{fl} = \frac{I_{fl}}{I_{std}} \frac{\sigma_{std}}{\sigma_a} \frac{c_{std}}{c_{azo}} \kappa \tag{5}$$

where I_{fl} is the integrated fluorescence intensity, I_{std} is the integrated Raman intensity of ethanol's CH stretch band at 2880 cm^{-1}, σ_{std} is the absolute Raman cross-section for the standard peak, σ_a is the absorption cross-section of azobenzene at the excitation wavelength (0.035 $Å^2$ for *cis*-azobenzene and 0.014 $Å^2$ for trans-azobenzene), and c_{std} and c_{azo} are the concentrations of ethanol and azobenzene, respectively. Additionally, a correction for the difference in the depolarization ratio between ethanol Raman and azobenzene fluorescence scattering must be applied and is given by

$$\kappa = \left(\frac{1+2\rho}{1+\rho}\right)_{fl} / \left(\frac{1+2\rho}{1+\rho}\right)_{std} \tag{6}$$

In the case of *trans*-azobenzene, the depolarization ratio, ρ, was measured to be $\sim 0.39 \pm 0.4$, resulting in κ equal to 1.2. Given the ultrashort lifetime of *cis*-azobenzene, the depolarization value is not expected to differ significantly from 0.33.

2.4. Strickler−Berg Analysis and Calculated Excited-State Lifetimes. The natural radiative lifetime τ_{rad} can be approximated by utilizing the absorption and fluorescence spectra according to the Strickler−Berg relationship:[40]

$$\tau_{rad}^{-1} = 2.88 \times 10^{-9} n^2 \langle \nu_f^{-3} \rangle_{av}^{-1} \int \epsilon \mathrm{d}(\ln \nu) \tag{7}$$

where n is the index of refraction, ϵ is the molar extinction coefficient, ν is the frequency in centimeters^{-1}, and $\langle \nu_f^{-3} \rangle_{av}^{-1}$ is calculated from the following equation:

$$\langle \nu_f^{-3} \rangle_{av}^{-1} = \int I_f(\nu) \mathrm{d}\nu / \int I_f(\nu) / \nu^3 \mathrm{d}\nu \tag{8}$$

where $I_f(\nu)$ is the fluorescence spectrum as a function of energy, ν. Using the natural radiative lifetime, the excited-state lifetime is estimated from

$$\Phi_{fl} = \tau / \tau_{rad} \tag{9}$$

3. Results

3.1. Raman Spectra of *cis*- and *trans*-Azobenzene. Raman spectra of azobenzene solutions with different cis and trans isomer compositions are compared in Figure 1. The isomer concentrations were changed by exposing predominantly cis samples to room light for 0, 5, 10, 25, and 60 min. The assignment of the cis and trans bands was made by comparison of peak intensity changes with compositional changes. Most obvious are the five intense bands at 275, 542, 594, 621, and 778 cm^{-1} that decrease dramatically as cis converts to trans. As the relative amount of cis decreases, a broad band at 1134 cm^{-1} decreases, and a sharper band centered at 1143 cm^{-1} grows in amplitude. The intensity of the 1512 cm^{-1} band decreases, and the band intensities at 1472 and 1492 cm^{-1} increase with the higher trans concentration. Additionally, the 1440 cm^{-1} band grows in as a shoulder on the residual ethanol peak at 1450 cm^{-1} with increased trans concentration.

Kinetic analysis of the Raman intensities of each azobenzene band as a function of exposure time allows bands to be assigned to either the cis or the trans isomer. Figure 2 shows isomer composition as a function of light exposure. With longer exposure times, more of the cis isomer converts to the trans conformation as shown in panel a of Figure 2. Fitting these points to a single-exponential function reveals a time constant of 0.13 s^{-1}. Analogous fits were obtained for the changes in Raman intensities as a function of time (panel b in Figure 2) for the 778 cm^{-1} cis and 1492 cm^{-1} trans bands. On the basis of this kinetic analysis, vibrational bands due solely to *cis*-azobenzene were 275, 542, 594, 621, 778, 1134, and 1512 cm^{-1}, and bands due to *trans*-azobenzene were 1000, 1143, 1183, 1440, 1472, and 1492 cm^{-1}. The 1592 cm^{-1} band has contributions from both isomers. Vibrational assignments for these modes (Tables 1 and 2) have been made based on our DFT calculations as well as literature values.[41]

3.2. Comparison of the Resonance Raman Features of *trans*- and *cis*-Azobenzene. The 406 nm resonance Raman spectra of pure *cis*- and *trans*-azobenzene obtained by subtracting the interfering isomer and solvent bands are presented in Figure 3. The most notable features of *trans*-azobenzene occur at 1143 cm^{-1} (CN stretch), 1440 cm^{-1} (NN stretch), 1472 cm^{-1} (CC stretch), and 1492 cm^{-1} (CC stretch). Smaller bands are also present at 1000, 1183, 1315, and 1592 cm^{-1} and correspond mostly to CC bends/stretches (Table 1). In contrast, the most intense peaks for *cis*-azobenzene occur at 275 cm^{-1} (CCNN torsion), 542 cm^{-1} (NNC bend), 594 cm^{-1} (CNNC torsion), and 778 cm^{-1} (CCCH torsion) with less intense bands occurring at 1134 cm^{-1} (CN stretch), 1512 cm^{-1} (NN stretch), and 1592 cm^{-1} (CC stretch). The band assignments of *cis*- and *trans*-azobenzene in Tables 1 and 2 reveal several interesting vibrational shifts. For example, the weak NN stretch is found

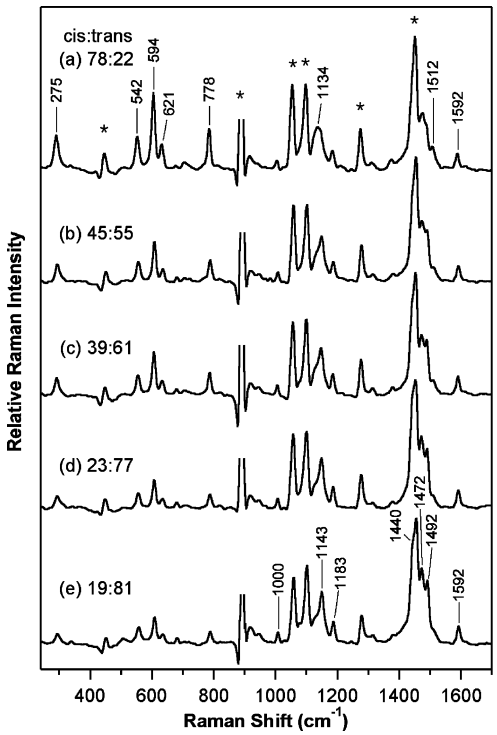

Figure 1. Resonance Raman spectra of mixtures of *cis*- and *trans*-azobenzene in ethanol. Various ratios of the cis and trans isomers were produced by exposing a previously prepared cis sample to room light for 0, 5, 10, 25, and 60 min (traces a−e, respectively). The ratios of the cis and trans isomers are (a) 78:22, (b) 45:55, (c) 39:61, (d) 23:77, and (e) 19:81 as determined by the absorption spectra. Spectra were acquired with 458 nm excitation, and ethanol solvent peaks were subtracted. The residual ethanol CO stretch peak (875−925 cm^{-1}) was truncated, and asterisks mark other residual solvent lines.

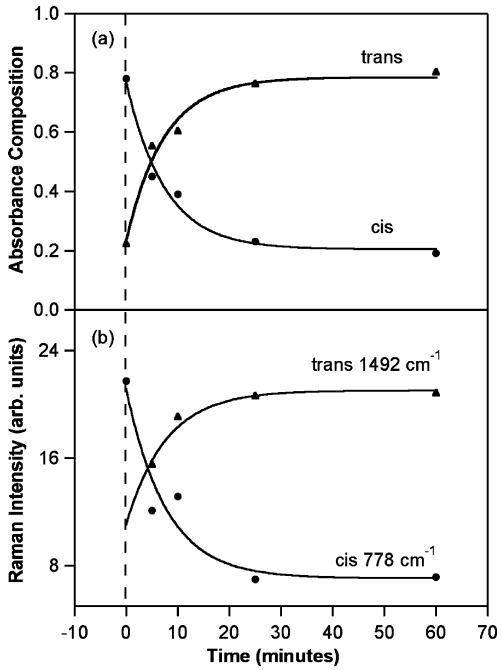

Figure 2. Analysis of azobenzene isomer composition as a function of exposure time to room light. Panel a shows the percentage of trans and cis isomers as a function of light exposure as determined by absorption spectra. The trans isomer exponentially grows in with a constant of 0.13 s^{-1}. Panel b shows the relative intensity of the exemplary 778 cm^{-1} *cis*-azobenzene and 1492 cm^{-1} *trans*-azobenzene bands as a function of time. The exponential fit to these points also provides a constant of 0.13 s^{-1}. On the basis of such a kinetic analysis, the various bands labeled in Figure 3 have been assigned to either *cis*- or *trans*-azobenzene. Error in the Raman intensity amounts to approximately 2% and is represented by the size of the symbols.

at 1512 cm^{-1} in *cis*-azobenzene and shifts to 1440 cm^{-1} in *trans*-azobenzene with much more intensity. The CN stretch also shifts from a broad band at 1134 cm^{-1} in *cis*-azobenzene to a more narrow band centered at 1143 cm^{-1} in *trans*-azobenzene.

The resonance Raman spectra of pure *trans*-azobenzene with excitation at 406, 458, 488, and 496 nm are compared in Figure 4. Spectra of the pure trans isomer were obtained by subtracting the bands due to the interfering isomer and solvent. The ethanol CO stretch band intensity before solvent subtraction has been included to show the internal standard used for calculations of the absolute cross-sections. Bands at 1143, 1440, 1472, and 1492 cm^{-1} show the greatest intensity with Raman cross-sections on the order of 10^{-10} $Å^2$/molecule (see Table 3). Less intense bands are also observed at 1000, 1183, 1315, and 1592 cm^{-1} with Raman cross-sections that are an order of magnitude lower. Excitation at 406 nm results in the largest cross-sections. Additionally, all bands are less intense than expected with excitation at 458 nm. This effect is likely due to interference with the second excited state (S_2) and is discussed in Section 4.3.

Resonance Raman spectra of cis-azobenzene at 406, 458, 488, and 496 nm excitation are compared in Figure 5. The low frequency bands at 275, 542, 594, 778, and 1134 cm^{-1} show the greatest intensities with cross-sections on the order of 10^{-10} $Å^2$/molecule (see Table 3). Three additional bands are observed for *cis*-azobenzene with less intensity at 621, 1514, and 1592 cm^{-1}. The most apparent differences between *cis*-azobenzene and *trans*-azobenzene are found in the 200−800 cm^{-1} region. The greater intensities of the low frequency bands for *cis*-azobenzene show that more low frequency torsional modes have significant FC displacements in the excited state.

TABLE 1: Excited-State Displacements and Mode Descriptions for *trans*-Azobenzene

exptl frequency (cm^{-1})	DFT calcd frequency (cm^{-1})	DFT character[a,b]	best fit delta[c]
1000	1015	δ(CCC)	0.18
1143	1169	ν(CN) + δ(CNN) + δ(NCC) + δ(CCH)	0.55
1183	1213	ν(CN) + δ(CNN) + δ(NCC) + δ(CCH)	0.23
1315	1340	δ(CCH) + δ(NCC)	0.13
1440	1558	ν(NN) + δ(CNN) + δ(NCC) + δ(CCH)	0.66
1472	1487	ν(NN) + ν(CN) + δ(CNN) + δ(NCC) + δ(CCH)	0.50
1492	1514	ν(CC) + δ(CCH) + ν(NN)	0.40
1594	1652	ν(CC) + ν(NN) + δ(CCH)	0.23

[a] τ = torsion, δ = in-plane bend, and ν = stretch. [b] τ(CCCH), δ(CCC), δ(CCH), and ν(CC) are motions within the phenyl rings. This labeling scheme represents several combinations of different atoms in the phenyl rings. [c] Indicated best-fit deltas are with Γ = 120 cm^{-1}, θ = 1490 cm^{-1}, E_0 = 21880 cm^{-1}, and M = 0.21 Å.

3.3. Raman Intensity Calculations. Raman intensity calculations were performed to quantify the FC coupling of the vibrational modes with S_1 electronic excitation. The displacements along the relevant vibrational modes for each isomer were optimized to reproduce their experimental Raman cross-sections (Table 3), while simultaneously fitting the experimental absorption spectrum. Using the parameters listed in Tables 1 and 2, the calculated (dotted) and experimental (dashed) absorption spectra are in excellent agreement (Figure 6). The absorption

TABLE 2: Excited-State Displacements and Mode Descriptions for *cis*-Azobenzene

exptl frequency (cm^{-1})	DFT calcd frequency (cm^{-1})	DFT character[a,b]	best fit delta[c]
275	288	τ(CCNN)	0.68
542	548	δ(NNC) + τ(NNCC) + τ(CCCC) + δ(CCC)	0.35
594	609	τ(CNNC) + τ(CCCH)	0.45
621	632	δ(CCC) + τ(CNNC)	0.24
778	788	τ(CCCH) + τ(CCCC) + τ(CNNC)	0.34
1134	1152	ν(CN) + δ(CCH)	0.31
1512	1605	ν(NN) + ν(CC) + δ(CCH)	0.15
1592	1642	ν(CC) + δ(CCH) + δ(CCC)	0.15

[a] τ = torsion, δ = in-plane bend, and ν = stretch. [b] τ(CCCH), δ(CCC), δ(CCH), and ν(CC) are motions within the phenyl rings. This labeling scheme represents several combinations of different atoms in the phenyl rings. [c] Indicated best-fit deltas are with $\Gamma = 900\ cm^{-1}$, $\theta = 1445\ cm^{-1}$, $E_0 = 22375\ cm^{-1}$, and $M = 0.35$ Å.

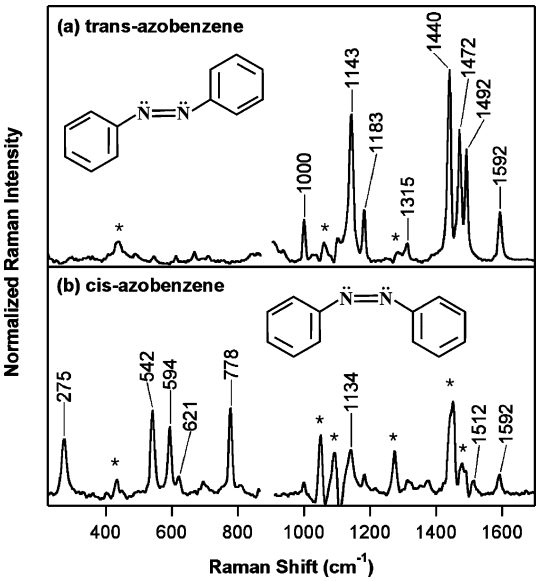

Figure 3. Comparison of pure *cis*- and *trans*-azobenzene Raman spectra in ethanol with 406 nm excitation. Spectra are presented after the interfering isomer and solvent bands have been subtracted. Spectra are normalized for azobenzene concentration, corrected for instrument response, and corrected for self-absorption. The residual CO stretch of ethanol has been removed for clarity.

cross-section for the weak S_0-S_1 ($n\pi^*$) transition for *cis*-azobenzene is approximately 2 times greater than that of *trans*-azobenzene.

Comparisons of the eight-mode Raman intensity calculation for *trans*-azobenzene with the experimental absolute resonance Raman cross-sections are shown in Figure 7. Deltas were adjusted to reproduce the resonance Raman cross-sections at 488 nm. For reasons discussed next, deltas were constrained using the 488 and 496 nm experimental Raman cross-sections. Several sets of deltas with different scalings were explored to simultaneously model the absorption and Raman profiles, while the homogeneous and inhomogeneous broadening parameters were adjusted to maintain a good fit to the absorption band. The deltas with the largest magnitude that resulted in good agreement between experimental and calculated absorption and Raman profiles employed a homogeneous broadening of 120 cm^{-1}. Attempts to use larger relative values for the displacements resulted in an absorption spectrum that was too broad, and this breadth could not be reduced by any set of homogeneous or inhomogeneous broadenings. In the absence of other

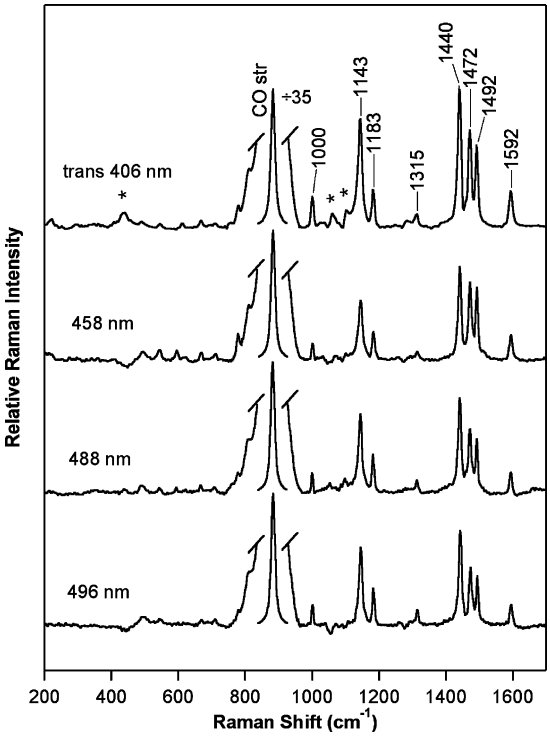

Figure 4. Resonance Raman spectra of *trans*-azobenzene in ethanol at the indicated excitation wavelengths. Spectra are presented after bands of the interfering isomer and solvent have been subtracted. The CO band at 881 cm^{-1} has been included (scaled by 35) to indicate the relative magnitude of the azobenzene peaks to the solvent CO stretch intensity before subtraction. All spectra are corrected for instrument response and self-absorption. Spectra are normalized to have the same intensity for the CO stretch at all excitation wavelengths. Asterisks mark residual solvent lines.

TABLE 3: Resonance Raman Cross-Sections for *trans*- and *cis*-Azobenzene[a,b]

trans-azobenzene frequency (cm^{-1})	σ_R at excitation wavelength (A^2/molecule $\times 10^{-10}$)			
	406 nm	458 nm	488 nm	496 nm
1000	0.47	0.20	0.15	0.19
1143	3.69	1.58	1.45	1.50
1183	0.67	0.40	0.37	0.41
1315	0.27	0.14	0.13	0.22
1440	3.94	2.01	1.50	1.60
1472	2.26	1.48	0.86	0.82
1492	1.55	1.05	0.54	0.54
1592	0.79	0.41	0.20	0.26
cis-azobenzene frequency (cm^{-1})	σ_R at excitation wavelength (A^2/molecule $\times 10^{-10}$)			
	406 nm	458 nm	488 nm	496 nm
275	2.30	1.40	0.45	0.45
542	2.39	1.09	0.29	0.22
594	1.61	2.10	1.01	0.97
621	0.32	0.62	0.27	0.22
778	2.04	1.62	0.31	0.20
1134	2.50	1.71	0.80	0.48
1512	0.37	0.41	0.25	0.19
1592	0.49	0.39	0.16	0.17

[a] Cross-sections of azobenzene were calculated using the CO stretch of ethanol as a reference peak. [b] Extrapolated cross-sections of ethanol's CO stretch at 406, 458, and 496 nm excitation are 6.4×10^{-14}, 3.9×10^{-14}, and 2.8×10^{-14} $Å^2$/molecule, respectively.

experimental criteria, the parameter set with the largest deltas was used for further analysis. The presented REPs for *trans*-azobenzene (Figure 7) employed homogeneous broadening of 120 cm^{-1} (fwhm), inhomogenous broadening of 1490 cm^{-1} (fwhm), $E_0 = 21880\ cm^{-1}$, and $M = 0.21$ Å. The results of the

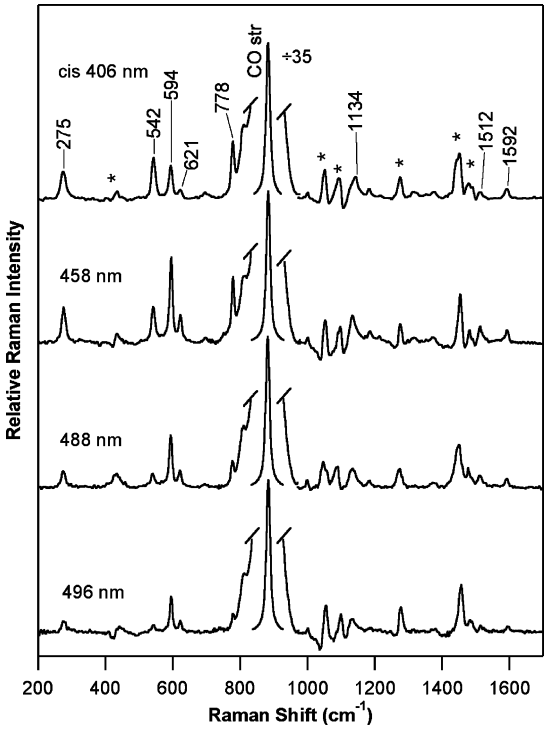

Figure 5. Resonance Raman spectra of *cis*-azobenzene in ethanol at the indicated excitation wavelengths. Spectra are presented after subtraction of residual trans and solvent bands to best display the vibrational bands of *cis*-azobenzene. The CO stretch of ethanol (scaled by a factor of 35) is included as a reference peak. All spectra are corrected for instrument response and self-absorption. Spectra are normalized to have the same intensity for the ethanol CO stretch at all excitation wavelengths. Asterisks mark residual solvent lines.

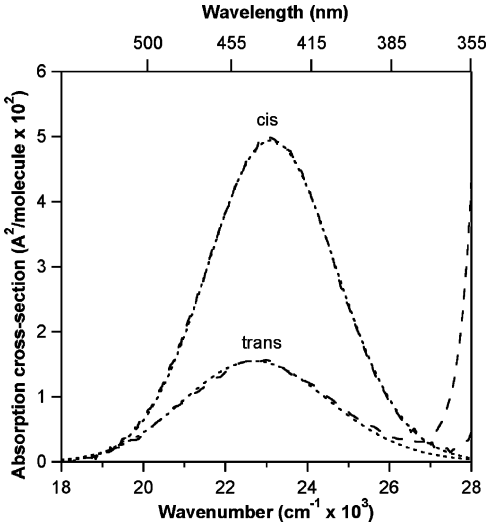

Figure 6. Comparison of the experimental and calculated absorption spectra for pure *trans*- and *cis*-azobenzene. Experimental absorption spectra of trans and cis are shown as dashed lines. Calculated absorption spectra of trans and cis are indicated with dotted lines using the parameters listed in Tables 1 and 2.

calculations presented in Table 1 indicate that for *trans*-azobenzene, the largest displacements of 0.66 and 0.55 are in the NN (1440 cm^{-1}) and CN (1143 cm^{-1}) stretching modes as expected. Error bars for the experimental cross-sections include errors in the integrated area of each band. Additionally, since some of the vibrational bands of each isomer overlap, an additional ~20% error due to the presence of the interfering isomer was estimated by evaluating the kinetic fit of cis to trans isomerization, such as is shown in Figure 2.

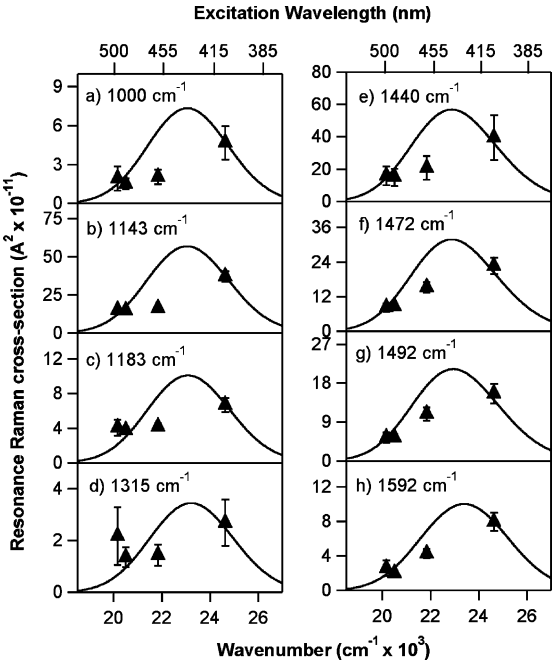

Figure 7. Comparison of Raman excitation profiles (solid lines) with the experimental cross-sections (points) for *trans*-azobenzene with $\Gamma = 120\ cm^{-1}$, $\theta = 1490\ cm^{-1}$, $E_0 = 21880\ cm^{-1}$, $M = 0.21$ Å, and deltas listed in Table 1. Error bars have been included for all points; however, in most cases, the errors are small as compared to the size of the marker.

The experimental cross-sections for the trans modes are systematically lower than the calculated REPs with 458 nm excitation. For the 1000 and 1143 cm^{-1} modes, the calculated cross-sections are a factor of 3 greater than the experimental cross-sections, while for other modes, the discrepancy is a factor of 2 at 458 nm. Since the errors in the experiment and the variance in the calculation are small as compared to this difference, we suggest that the differences are real and likely a result of interference effects with the S_2 state ($\pi\pi^*$ transition, $\lambda_{max} = 317$ nm).

Analogous calculations (Figure 8) were carried out for *cis*-azobenzene using eight modes to model the absorption and Raman cross-sections. The 458 nm resonance Raman cross-sections were used to constrain the relative deltas, and the final synthesis reproduced the cross-sections at all excitation wavelengths with the exception of 406 nm, which is discussed below. Several sets of deltas with different scaling were used to simultaneously model the absorption and Raman data, while the homogeneous and inhomogeneous broadening parameters were adjusted to maintain a good fit to the absorption. The largest set of deltas that resulted in good agreement between experimental and calculated absorption and Raman profiles required a homogeneous broadening of 900 cm^{-1}. Attempts to use even larger deltas resulted in an absorption spectrum that was too broad; analyses with delta sets of smaller magnitude and larger homogeneous broadening are less physically realistic. We have chosen to use the parameter set with homogeneous broadening of 900 cm^{-1} (fwhm), inhomogeneous broadening of 1445 cm^{-1} (fwhm), $E_0 = 22375\ cm^{-1}$, and $M = 0.35$ Å for further analysis because it constitutes an upper limit for the deltas. The modes with the greatest displacements for *cis*-azobenzene are the CCNN torsion ($\Delta = 0.68$) and the CNNC torsion ($\Delta = 0.45$) at 275 and 594 cm^{-1}, respectively (Table 2).

The calculated intensities for many of the *cis*-azobenzene bands (594, 621, 1512, and 1592 cm^{-1}) at 406 nm are 2−4-fold higher than the experimental values. The experimental

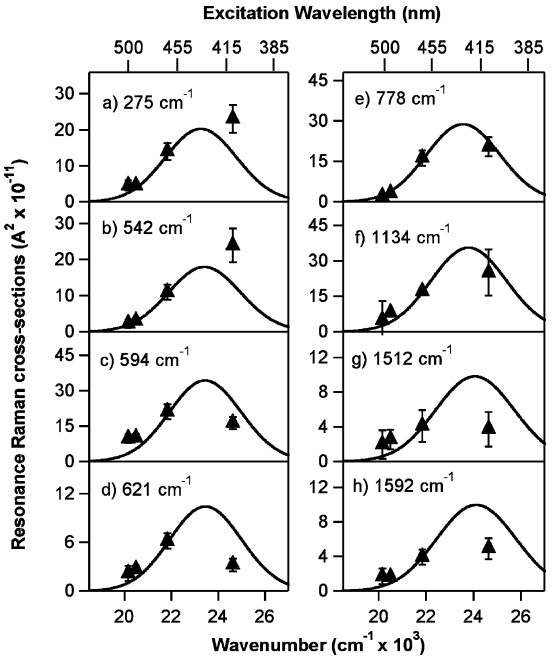

Figure 8. Comparison of the calculated Raman excitation profiles (solid lines) with experimental cross-sections (points) of *cis*-azobenzene with $\Gamma = 900$ cm^{-1}, $\theta = 1445$ cm^{-1}, $E_0 = 22375$ cm^{-1}, $M = 0.35$ Å, and deltas listed in Table 2. Error bars have been included for all data points but are small compared to the symbol size.

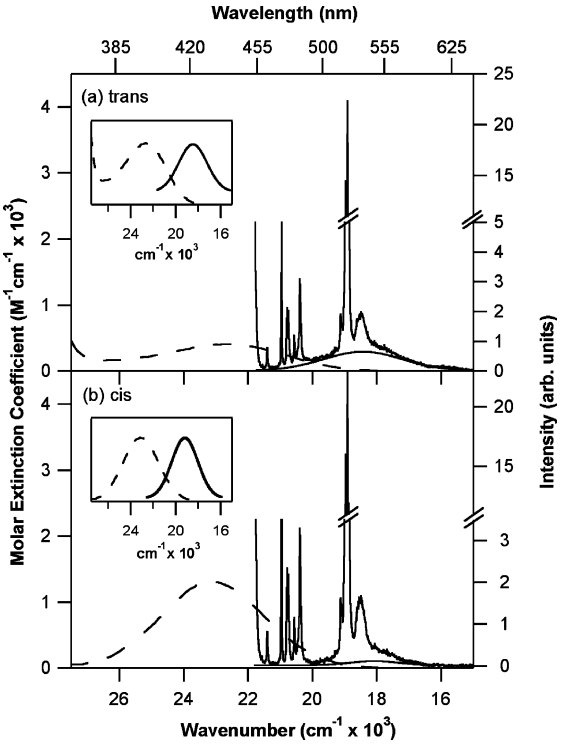

Figure 9. Absorption and emission spectra of azobenzene in ethanol. Panel a shows sharp Raman features of *trans*-azobenzene and ethanol on top of a broad background due to trans fluorescence. The absorption spectrum of *trans*-azobenzene is also shown as a dashed line. Panel b shows Raman features of *cis*-azobenzene and ethanol on top of a weak background due to cis fluorescence. The absorption spectrum of *cis*-azobenzene is also shown as a dashed line. The insets display the absorption and emission spectra with appropriate scaling factors to show mirror symmetry. Spectra were acquired with 458 nm excitation.

errors are small as compared to this variance, indicating that the decreased intensities at 406 nm are significant. However, the 275 and 542 cm^{-1} modes (traces a and b in Figure 8) show calculated intensities that are ~2 times less than the experimental intensities. All calculated REPs are well-fit to the Raman cross-sections at the three lowest excitation energies.

3.4. Azobenzene Fluorescence Quantum Yield. Fluorescence spectra of *trans*-azobenzene excited at 458 nm are presented in Figure 9a. The sharp bands around 480−500 and 520−560 nm are due to the Raman features of ethanol. The broad background ranging from ~460−600 nm is attributed to the fluorescence of *trans*-azobenzene and is peaked at ~530 nm. Using the absorption cross-section of 0.14 Å^2 at 458 nm and the CH stretch as the standard, the fluorescence quantum yield for *trans*-azobenzene is found to be $(1.1 \pm 0.1) \times 10^{-5}$. From Strickler−Berg analysis (eqs 6−9), the natural radiative lifetime is $\tau_{rad} = 300$ ns, resulting in an estimated excited-state lifetime of ~3 ps.

Figure 9b presents the emission spectrum of *cis*-azobenzene with 458 nm excitation. The sharp Raman features of ethanol are evident, while the broad fluorescence background is very weak. Subtraction of the trans contribution from the cis spectrum results in a weak curve with an amplitude that is ~10% that of the trans fluorescence spectrum. The cis fluorescence quantum yield after correction for the trans component is $\sim 1 \times 10^{-6}$, which corresponds to an excited-state lifetime of ~200 fs using the calculated 180 ns radiative lifetime.

4. Discussion

Despite many experiments and calculations aimed at understanding the isomerization dynamics of azobenzene, there is still uncertainty concerning the mechanisms and rates of the isomerization processes. Most studies have been performed on *trans*-azobenzene due to its stability and accessible picosecond isomerization dynamics. Additional difficulty arises for *cis*-azobenzene because it isomerizes on the femtosecond time scale, making direct observation more challenging. Here, we obtain information on the excited-state structural dynamics for both isomers by modeling the absorption and Raman cross-sections to determine the ground- to excited-state geometry changes and discuss the implications of our results on possible isomerization pathways. To obtain a more complete picture of the excited-state dynamics, the fluorescence quantum yields were also measured, and the excited-state lifetimes were estimated from Strickler−Berg analysis.

4.1. Excited-State Dynamics of *trans*-Azobenzene. The initial excited-state motions along internal coordinates were determined using the FC displacements from Raman intensity analysis. The rotation pathway should exhibit initial changes along the CNNC torsional modes, while the inversion pathway should involve motion along the CNN bend internal coordinate. One difficulty in analyzing the excited-state structural changes from resonance Raman intensity analysis is the sign ambiguity for each of the displacements. For eight displaced modes, there are 2^8 possible sign combinations. To simplify the discussion, we focus on displaced normal modes with significant contributions from the CNN bend or CNNC torsion as determined using Gaussian 03.[39] Exploring all the sign combinations of the four modes with the most CNN bend character (1143, 1183, 1440, and 1472 cm^{-1}) reveals that the CNN bend angle at the harmonic minimum changes in the excited state by 0.4 to 6° for relative phases of $+ - + +$ to $+ + - -$, respectively. In comparison, the CN bond length shows at most a 0.3% change (0.004 Å), and the NN bond changes at most 0.2% (0.003 Å). A strong correlation between CNN angle and CN bond length was also found for all sign combinations; if the CN bond shortens (as expected for π^* excitation), the CNN angle

increases. Changes in the CN and NN bonds were also correlated such that shortening the CN bond resulted in elongation of the NN bond. Although the phases cannot be unambiguously determined from our data alone, large changes in the CNN bend and CN stretching coordinates in the excited state are consistent with motions along the inversion coordinate, in agreement with previous work.[23,30] Additionally, *trans*-azobenzene remains remarkably planar with no appreciable changes along the dihedral angles using any sign combination. Our results support the idea that isomerization occurs via inversion for *trans*-azobenzene.

Although a significant amount of work has been performed to determine the excited-state dynamics of *trans*-azobenzene, the question of the S_1 lifetime for *trans*-azobenzene is still debated. Our measured fluorescence quantum yield of 1.1×10^{-5} predicts an excited-state lifetime of 3 ps using Strickler−Berg analysis. Transient absorption experiments of azobenzene in ethanol, DMSO, and *n*-hexane following $n\pi^*$ excitation have found an S_1 lifetime of ∼2−3 ps,[17,18,20] while early picosecond time-resolved fluorescence measurements in cyclohexane have assigned the S_1 excited-state lifetime an upper limit of ∼30 ps.[16] The lifetime and reaction pathways are also known to depend strongly on solvent viscosity varying from 1 ps in *n*-hexane to 12.5 ps in ethylene glycol as found by picosecond time-resolved Raman and femtosecond fluorescence anisotropy studies.[19,21] Our predicted excited-state lifetime of 3 ps from Strickler−Berg analysis is in good agreement with previous direct measurements of the S_1 lifetime using transient absorption techniques.

4.2. Excited-State Dynamics of *cis*-Azobenzene. Initial isomerization dynamics of *cis*-azobenzene are determined by calculating the displacements along each internal coordinate using eq 4. Three normal modes of *cis*-azobenzene (594, 621, and 778 cm^{-1}) have significant contributions from the CNNC torsion internal coordinate, and there are eight possible sign combinations that affect the magnitude of the predicted harmonic CNNC dihedral angle change. Using these combinations, excited-state CNNC dihedral angle changes in *cis*-azobenzene were found to range from 6 to 20° for phase combinations of + + + and + − −, respectively. The 6−20° CNNC dihedral angle change found for *cis*-azobenzene is very significant since no such change is found for *trans*-azobenzene. On the basis of this observation, there is significant initial excited-state motion along the torsional coordinate. Because the molecule is nonplanar in the ground state,[10−13] it experiences a nonzero slope along the non totally symmetric torsional degrees of freedom in the FC region as evidenced by the intensity of low frequency modes and has a strong preference for twisting.

If it is assumed that the isomerization proceeds via torsional degrees of freedom, the NN torsional mode at 594 cm^{-1} can be modeled as a linear potential of the form $V = -\beta q$. This model is based on the idea that motion along this coordinate is essentially dissociative; as the wavepacket moves away from the FC region, it has sufficient coupling to the ground state and does not return to the FC region. Using $\omega = 594$ cm^{-1} and $\Delta = 0.45$ for the NN torsion, the slope, β, of the excited-state surface in the FC region is calculated to be 270 cm^{-1}. The position of the center of the wavepacket at time t in dimensionless coordinates is estimated by:[14]

$$q(t) = \beta\omega t^2/2\hbar^2 \qquad (10)$$

A dimensionless displacement of $q = 1$ corresponds to a CNNC dihedral angle of ∼5°.[42] Using eq 10, a dihedral angle of 90° (approximate angle at the conical intersection)[26−31] corresponding to $q = 16$ is reached in only 80 fs, which is in good agreement with calculations and transient absorption experiments suggesting an excited-state lifetime of ∼100−170 fs.[17,20,30]

The fluorescence quantum yield of *cis*-azobenzene is very weak, suggesting that it has a subpicosecond excited-state lifetime. The cis fluorescence quantum yield is measured to be $\sim 1 \times 10^{-6}$ and predicts an excited-state lifetime of ∼200 fs. This value is nicely consistent with direct measurements from transient absorption experiments providing a 170 fs excited-state lifetime in ethanol.[17]

From this analysis, it is clear that the initial nuclear dynamics of *cis*- and *trans*-azobenzene are significantly different. The excited-state dynamics can be partially understood in terms of the ground-state geometries. In the case of *cis*-azobenzene, the molecule is sterically hindered by the phenyl group, which results in the central double bond being twisted by 10°, thereby priming the isomerization. This symmetry reduction results in a significant FC slope along torsional modes, providing a driving force for the isomerization to occur in hundreds of femtoseconds. *trans*-Azobenzene, on the other hand, is planar in both the ground state and the initially prepared excited state and isomerizes in 10 ps. The early time dynamics do not show evidence of motion along the rotational coordinate; this implicates a much slower inversion coordinate as the primary isomerization pathway.

4.3. Resonance Deenhancement. While the calculated Raman excitation profiles of *trans*- and *cis*-azobenzene provide a good fit to the experimental cross-sections, considerable differences between calculated profiles and experimental cross-sections are apparent for *trans*- and *cis*-azobenzene at 458 and 406 nm excitation, respectively. A likely explanation for this result is Raman deenhancement, caused by destructive interference of Raman scattering from two different electronic states. Our experiments probe the ∼450 nm bands corresponding to S_1 excitation ($n\pi^*$); however, the S_2 ($\pi\pi^*$) bands at 317 nm for *trans*-azobenzene and ∼280 nm for *cis*-azobenzene have oscillator strengths that are significantly greater. Therefore, as suggested by Umapathy's previous resonance Raman studies of *trans*-azobenzene, cross-terms that arise from the interaction of the S_1 and S_2 polarizabilities may be significant for certain modes.[23] Interference in resonance Raman scattering is possible when there is an additional interfering excited state above or near the resonant state of interest. In the perturbative limit, this interfering excited state may lie close to the resonant state and have a similar polarizability, but if it has a significantly larger polarizability than the state of interest, then they must be sufficiently separated in energy so that the higher energy state does not dominate the scattering. Additionally, there must be significant displacements in modes common to both excited states.[43] In cases where the transition dipole moment of the interfering state is large and the energies are well-separated, it has been found that the maximum interference occurs near the energy maximum of the resonant absorption band.[43,44] However, the magnitude and position of the deenhancement in the REPs also depend on the magnitude and direction of deltas in each of the excited states.

Raman excitation profiles of *trans*-azobenzene (Figure 7) show evidence of deenhancement in all vibrational bands at 458 nm. The S_1 and S_2 excited states of *trans*-azobenzene are separated by ∼9000 cm^{-1}, and the S_2 state has an oscillator strength that is ∼40 times greater than that of S_1.[1] Since we observe deenhancement for all modes, it is likely that these modes are FC coupled in both excited states. In fact, RR spectra acquired with an S_2 resonant probe (336−366 nm) have shown

that all the same vibrational bands are Raman active.[45] Our results contrast with those of previous RR intensity analyses of *trans*-azobenzene probed in the S_1 band that showed deenhancement only in the 1000, 1142, 1181, 1312, and 1439 cm^{-1} modes.[23,46] We are uncertain of the reason for this discrepancy.

Raman excitation profiles of *cis*-azobenzene (Figure 8) show experimentally lower cross-sections at 406 nm than predicted from Raman intensity analyses for the 594, 621, 1512, and 1592 cm^{-1} modes, while the experimental cross-sections are higher than predicted by the REPs of the 275 and 542 cm^{-1} modes at 406 nm excitation. In the case of *cis*-azobenzene, the S_1 and S_2 states are separated by $\sim$14 000 cm^{-1}, and S_2 has an oscillator strength approximately 4 times greater than that of the S_1.[1] For systems exhibiting interference effects with a preresonant state, the shape of the REPs is found to depend strongly on the signs of the deltas in the two excited states.[43,47] Thus, one possibility is that the differences in the REPs of the 275 and 542 cm^{-1} modes can be attributed to different sign combinations for the displacements in the two excited states as compared to the other modes, showing destructive interference.

5. Conclusion

Resonance Raman spectra of *cis*- and *trans*-azobenzene were acquired in resonance with the S_1 electronic transition. Clear differences in the spectra of each isomer were observed: *cis*-azobenzene exhibits strong low frequency torsional modes, while *trans*-azobenzene has intense skeletal stretching and bending modes. Resonance Raman intensity analysis reveals that upon excitation, the initial structural changes of *trans*-azobenzene are localized in the CNN bend and CN and NN stretches, consistent with an inversion mechanism. In contrast, *cis*-azobenzene exhibits large displacements along the CNNC torsion, showing that torsional motion contributes to the early time dynamics. These differences are attributed to the fact that the ground state of *cis*-azobenzene is sterically twisted, thereby priming the molecule for isomerization via rotation, as was found for *cis*-stilbene.[14] The excited-state torsional slope as well as the $\sim$200 fs S_1 lifetime for *cis*-azobenzene both suggest a steep and barrierless reaction coordinate that facilitates ultrafast rotational isomerization.

Acknowledgment. We thank Anne Myers Kelley for the RRModel program used to determine the ground- to excited-state dimensionless displacements. We also thank Dan Wandschneider for the ic_out program used to determine the A matrix elements. This work was supported by the Mathies Royalty Fund.

References and Notes

(1) Rau, H. Azo compounds. In *Photochromism: Molecules and Systems*; Durr, H., Bouas-Laurent, H., Eds.; Elsevier: New York, 1990.
(2) Ikeda, T.; Tsutsumi, O. *Science (Washington, DC, U.S.)* **1995**, *268*, 1873.
(3) Volgraf, M.; Gorostiza, P.; Numano, R.; Kramer, R. H.; Isacoff, E. Y.; Trauner, D. *Nat. Chem. Biol.* **2006**, *2*, 47.
(4) Renner, C.; Kusebauch, U.; Loweneck, M.; Milbradt, A. G.; Moroder, L. *J. Peptide Res.* **2005**, *65*, 4.
(5) Renner, C.; Moroder, L. *ChemBioChem* **2006**, *7*, 869.
(6) Yu, Y. L.; Nakano, M.; Ikeda, T. *Nature (London, U.K.)* **2003**, *425*, 145.
(7) Bortolus, P.; Monti, S. *J. Phys. Chem.* **1979**, *83*, 648.
(8) Rau, H.; Lüddecke, E. *J. Am. Chem. Soc.* **1982**, *104*, 1616.
(9) Siampiringue, N.; Guyot, G.; Monti, S.; Bortolus, P. *J. Photochem.* **1987**, *37*, 185.
(10) Mostad, A.; Romming, C. *Acta Chem. Scand.* **1971**, *25*, 3561.
(11) Kurita, N.; Tanaka, S.; Itoh, S. *J. Phys. Chem. A* **2000**, *104*, 8114.
(12) Fliegl, H.; Kohn, A.; Hattig, C.; Ahlrichs, R. *J. Am. Chem. Soc.* **2003**, *125*, 9821.
(13) Gagliardi, L.; Orlandi, G.; Bernardi, F.; Cembran, A.; Garavelli, M. *Theor. Chem. Acc.* **2004**, *111*, 363.
(14) Myers, A. B.; Mathies, R. A. *J. Chem. Phys.* **1984**, *81*, 1552.
(15) Curtin, D. Y.; Grubbs, E. J.; McCarty, C. G. *J. Am. Chem. Soc.* **1966**, *88*, 2775.
(16) Struve, W. S. *Chem. Phys. Lett.* **1977**, *46*, 15.
(17) Nägele, T.; Hoche, R.; Zinth, W.; Wachtveitl, J. *Chem. Phys. Lett.* **1997**, *272*, 489.
(18) Lednev, I. K.; Ye, T. Q.; Matousek, P.; Towrie, M.; Foggi, P.; Neuwahl, F. V. R.; Umapathy, S.; Hester, R. E.; Moore, J. N. *Chem. Phys. Lett.* **1998**, *290*, 68.
(19) Fujino, T.; Tahara, T. *J. Phys. Chem. A* **2000**, *104*, 4203.
(20) Satzger, H.; Sporlein, S.; Root, C.; Wachtveitl, J.; Zinth, W.; Gilch, P. *Chem. Phys. Lett.* **2003**, *372*, 216.
(21) Chang, C. W.; Lu, Y. C.; Wang, T. T.; Diau, E. W. G. *J. Am. Chem. Soc.* **2004**, *126*, 10109.
(22) Satzger, H.; Root, C.; Braun, M. *J. Phys. Chem. A* **2004**, *108*, 6265.
(23) Biswas, N.; Umapathy, S. *J. Chem. Phys.* **1997**, *107*, 7849.
(24) Cattaneo, P.; Persico, M. *Phys. Chem. Chem. Phys.* **1999**, *1*, 4739.
(25) Monti, S.; Orlandi, G.; Palmieri, P. *Chem. Phys.* **1982**, *71*, 87.
(26) Ishikawa, T.; Noro, T.; Shoda, T. *J. Chem. Phys.* **2001**, *115*, 7503.
(27) Cembran, A.; Bernardi, F.; Garavelli, M.; Gagliardi, L.; Orlandi, G. *J. Am. Chem. Soc.* **2004**, *126*, 3234.
(28) Ciminelli, C.; Granucci, G.; Persico, M. *Chem.—Eur. J.* **2004**, *10*, 2327.
(29) Diau, E. W. G. *J. Phys. Chem. A* **2004**, *108*, 950.
(30) Toniolo, A.; Ciminelli, C.; Persico, M.; Martínez, T. J. *J. Chem. Phys.* **2005**, *123*.
(31) Crecca, C. R.; Roitberg, A. E. *J. Phys. Chem. A* **2006**, *110*, 8188.
(32) Lu, Y. C.; Diau, E. W. G.; Rau, H. *J. Phys. Chem. A* **2005**, *109*, 2090.
(33) Hartley, G. S. *J. Chem. Soc.* **1938**, 633.
(34) Sokalski, W. A.; Gora, R. W.; Bartkowiak, W.; Kobylinski, P.; Sworakowski, J.; Chyla, A.; Leszczynski, J. *J. Chem. Phys.* **2001**, *114*, 5504.
(35) Stuart, C. M.; Tauber, M. J.; Mathies, R. A. *J. Phys. Chem. A* **2007**, *111*, 8390.
(36) Colles, M. J.; Griffith, J. E. *J. Chem. Phys.* **1972**, *56*, 3384.
(37) Lee, S. Y.; Heller, E. J. *J. Chem. Phys.* **1979**, *71*, 4777.
(38) Myers, A. B.; Mathies, R. A. A probe of excited-state structure and dynamics. In *Biological Applications of Raman Spectroscopy: Resonance Raman Spectra of Polyenes and Aromatics*; Spiro, T. G., Ed.; John Wiley and Sons: New York, 1987; Vol. 2, p 1.
(39) Frisch, M. J.; Trucks, G. W.; Schlegel, H. B.; Scuseria, G. E.; Robb, M. A.; Cheeseman, J. R.; Montgomery, J. A., Jr.; Vreven, T.; Kudin, K. N.; Burant, J. C.; Millam, J. M.; Iyengar, S. S.; Tomasi, J.; Barone, V.; Mennucci, B.; Cossi, M.; Scalmani, G.; Rega, N.; Petersson, G. A.; Nakatsuji, H.; Hada, M.; Ehara, M.; Toyota, K.; Fukuda, R.; Hasegawa, J.; Ishida, M.; Nakajima, T.; Honda, Y.; Kitao, O.; Nakai, H.; Klene, M.; Li, X.; Knox, J. E.; Hratchian, H. P.; Cross, J. B.; Bakken, V.; Adamo, C.; Jaramillo, J.; Gomperts, R.; Stratmann, R. E.; Yazyev, O.; Austin, A. J.; Cammi, R.; Pomelli, C.; Ochterski, J. W.; Ayala, P. Y.; Morokuma, K.; Voth, G. A.; Salvador, P.; Dannenberg, J. J.; Zakrzewski, V. G.; Dapprich, S.; Daniels, A. D.; Strain, M. C.; Farkas, O.; Malick, D. K.; Rabuck, A. D.; Raghavachari, K.; Foresman, J. B.; Ortiz, J. V.; Cui, Q.; Baboul, A. G.; Clifford, S.; Cioslowski, J.; Stefanov, B. B.; Liu, G.; Liashenko, A.; Piskorz, P.; Komaromi, I.; Martin, R. L.; Fox, D. J.; Keith, T.; Al-Laham, M. A.; Peng, C. Y.; Nanayakkara, A.; Challacombe, M.; Gill, P. M. W.; Johnson, B.; Chen, W.; Wong, M. W.; Gonzalez, C.; Pople, J. A.; *Gaussian 03*; Gaussian, Inc.: Pittsburgh, PA, 2004.
(40) Strickler, S. J.; Berg, R. A. *J. Chem. Phys.* **1962**, *37*, 814.
(41) Biswas, N.; Umapathy, S. *J. Phys. Chem. A* **1997**, *101*, 5555.
(42) The value of 5° is based on $\delta_i = 5.8065(A_{ji}\omega_j^{-1/2}\Delta_j)$ using $\Delta = 1$ for the 594 cm^{-1} mode since it has the most CNNC torsional character.
(43) Shin, K. S. K.; Zink, J. I. *J. Am. Chem. Soc.* **1990**, *112*, 7148.
(44) Hildebrandt, P.; Tsuboi, M.; Spiro, T. G. *J. Phys. Chem.* **1990**, *94*, 2274.
(45) Biancalana, A.; Campani, E.; Didomenico, G.; Gorini, G.; Masetti, G. *J. Raman Spectrosc.* **1993**, *24*, 43.
(46) Biswas, N.; Umapathy, S. *Chem. Phys. Lett.* **1995**, *236*, 24.
(47) Zgierski, M. Z. *J. Raman Spectrosc.* **1977**, *6*, 53.